fluids

MDPI

Article

High-Salinity Fluid Downslope Flow on Regolith Layer Examined by Laboratory Experiment: Implications for Recurring Slope Lineae on Martian Surfaces

Yoshiki Tabuchi [1], Arata Kioka [1,2,3,*], Takeshi Tsuji [3] and Yasuhiro Yamada [1,2]

[1] Cooperative Program for Resources Engineering, Graduate School of Engineering, Kyushu University, Fukuoka 819-0395, Japan
[2] Department of Earth Resources Engineering, Faculty of Engineering, Kyushu University, Fukuoka 819-0395, Japan
[3] School of Engineering, The University of Tokyo, Tokyo 113-8656, Japan
* Correspondence: kioka@sys.t.u-tokyo.ac.jp; Tel.:+81-3-5841-8683

Abstract

Numerous dark linear recurrent features called Recurring Slope Lineae (RSL) are observed on Martian surfaces, hypothesized as footprints of high-salinity liquid flow. This paper experimentally examined this "wet hypothesis" by analyzing the aspect ratios (length/width) of the flow traces on the granular material column to investigate how they vary with the granular material column, liquid and its flow rate, and inclination. While pure water produced low aspect ratios (<1.0) on the Martian regolith simulant column, high-salinity fluid ($CaCl_2$(aq)) traces exhibited significantly higher aspect ratios (>4.0), suggesting that pure water alone is insufficient to explain RSL formulation. Furthermore, the aspect ratios of high-salinity fluid traces on Martian regolith simulants were among the highest observed across all studied granular materials with similar particle sizes, aligning closely with actual RSL observed on Martian slopes. The results further suggest that variable ARs of actual RSL at the given slope can partly be explained by variable flow rates of high-salinity flow as well as salinity (i.e., viscosity) of flow. The results can be attributed to the unique granular properties of Martian regolith, characterized by the lowest permeability and Beavers–Joseph slip coefficient among the studied granular materials. This distinctive microstructure surface promotes surface flow over Darcy flow within the regolith column, leading to a narrow and long-distance feature with high aspect ratios observed in Martian RSL. Thus, our findings support that high-salinity flows are the primary driver behind RSL formation on Mars. Our study suggests the presence of salts on the Martian surface and paves the way for further investigation into RSL formulation processes.

Keywords: regolith; Mars; viscous downslope flow; Recurring Slope Lineae; Beavers–Joseph boundary condition

check for updates

Academic Editors: Pavel S. Berloff and Jean Reinaud

Received: 8 June 2025
Revised: 7 July 2025
Accepted: 11 July 2025
Published: 12 July 2025

Citation: Tabuchi, Y.; Kioka, A.; Tsuji, T.; Yamada, Y. High-Salinity Fluid Downslope Flow on Regolith Layer Examined by Laboratory Experiment: Implications for Recurring Slope Lineae on Martian Surfaces. *Fluids* **2025**, *10*, 183. https://doi.org/10.3390/fluids10070183

Copyright: © 2025 by the authors. Licensee MDPI, Basel, Switzerland. This article is an open access article distributed under the terms and conditions of the Creative Commons Attribution (CC BY) license (https://creativecommons.org/licenses/by/4.0/).

1. Introduction

Mars, once a warm, wet, and more dynamic planet, now presents a cold and arid landscape. Evidence of past fluvial activity, such as ancient riverbeds, lakebeds, and river delta formations, suggests Mars once possessed a more hospitable environment [1–4]. While liquid water is currently limited on the Martian surface, it may exist in various forms. Water ice is most likely present within the polar caps and permafrost [5–8], and extensive evidence has unveiled the presence of brines or hydrated salts [9,10]. High-salinity fluids

are more stable than pure water in such environments by decreasing the freezing point and evaporation rate of liquid [11–14]. The salts, such as chloride and perchlorate salts, are thus able to exist in liquid brine forms on and beneath the Martian surface by absorbing atmospheric water vapor through deliquescence [15–17]. The presence of these brines on the surface and subsurface has significant implications for the present and future potential habitability on Mars [18,19]. Understanding the distribution and behavior of water and salts on Mars is thus crucial for unraveling the planet's past, assessing its current state, and guiding future exploration missions.

On Mars, numerous dark linear recurrent features, called Recurring Slope Lineae (RSL), are observed on the surfaces [13]. The RSL is predominantly found on steep slopes (20–50°) in the low to mid-latitudes of the southern hemisphere [20]. The confirmed RSL forms during spring and summer and fades during autumn and winter [21]. There are two main hypotheses regarding the formation process of RSL: the "slope failure hypothesis" and "wet hypothesis." The first hypothesis is based on the slope failure processes due to the suspension of regolith (Mar's soil) caused by aeolian processes, sandstorms, or ascending gas current driven by warming gas molecules within the regolith column [21,22], leading to exposure to the bedrock and forming dark patterns. The hypothesis aligns with the known angle of repose of regolith and agrees well with the slope angles where RSL is present on the Martian surfaces [22,23]. Yet, the processes that would explain the seasonal occurrence and disappearance of RSL, as well as the presence of hydrate salts within RSL, remain unclear [9,24]. On the other hand, the "wet hypothesis" posits that the rise in temperature causes the deliquescence of salts or the emergence of groundwater, leading to the formation of RSL as downslope fluid flow [13,21]. In this hypothesis, the dark patterns are thought to be due to the discoloration of regolith-containing fluids, and the disappearance of RSL can also be explained by drying. A study comparing the elongation rate of RSL with the speed of fluid infiltration using Darcy's law found that the estimated permeability is consistent with the properties of Martian regolith [25]. Numerous studies have found observational evidence for the wet hypothesis; however, none of the definitive publications have studied the wet hypothesis through experiments, hampering a better understanding of the formation process of Martian RSL.

To deepen our understanding of RSL formation processes, this paper performs laboratory experiments studying high-salinity downslope liquid flow on the Martian regolith. The focus is on examining the wet hypothesis that brine liquid forms RSL. In the fields of fluid mechanics and granular physics, previous theoretical, experimental, and numerical works have explored the interaction between fluid flow in a porous medium and free flow [26–29]. However, none of these approaches have been used to study the RSL formation processes. The primary chemical compositions of salts composing RSL remain controversial; previous studies propose that calcium chloride, perchlorates, and sulfates generate surface flows [9,30–34]. Among the proposed salts, the shallow subsurface of Mars is enriched with calcium chloride ($CaCl_2$), which is also right with the eutectic temperature if RSL is from melting shallow frozen brines [30–34]. Therefore, this paper conducts a series of laboratory experiments of high-salinity $CaCl_2$(aq) downslope liquid flow on the Martian regolith simulant media. We analyzed the aspect ratio (ratio of length to width) of the generated high-salinity flow traces on the studied granular material column to investigate how they vary with the granular material column, liquid and its flow rate, and inclination. The results show that the high-salinity fluid flow and the distinctive properties of the underlying Martian regolith are vital for RSL formation processes. Our first-ever experimental study supports that high-salinity flows are the primary driver behind RSL formation on Mars, suggesting the presence of salts on the Martian surface and opening the door for further investigation into RSL formation.

2. Methods

2.1. Materials

We conducted a series of laboratory experiments to reproduce RSL formation in light of the high-salinity liquid flow hypothesis. We tested two different liquids, H_2O (pure water) and $CaCl_2$ (FUJIFILM Wako Pure Chemical Corp., Osaka, Japan) solution with 4.5 mol/kg (solubility 50%), with flow rates of 1.8 g/min and 2.5 g/min. The use of $CaCl_2$ is because it is a common substance with deliquescent properties and is the substance that can be present on the Martian surface [31,33,34] and probably forming RSL [9,13,33,35,36]. The eutectic concentration of $CaCl_2$ in the water system is 29–30 wt%, which is similar to that of other proposed salts such as $MgCl_2$ [37]. As testing granular materials, we used high-fidelity simulants of Martian global regolith (MGS-1) and lunar highlands regolith (LHS-1) [38–40] as well as terrestrial fine silica sand (T-8) in the experiments (Table 1). The Martian regolith simulant MGS-1 (Exolith Lab., Orlando, FL, USA) is created based on the exploration results from Curiosity, making it more reproducible compared to the commonly used Johnson Space Center JSC Mars-1 and Mojave Mars Simulant (MMS) [38]. The lunar regolith simulant LHS-1 (Exolith Lab., Orlando, FL, USA) and terrestrial silica sand T-8 (TOHOKU KEISYA Co., Ltd., Yamagata, Japan) were also tested for comparison purposes to better characterize RSL formation on Martian granular media. Scanning Electron Microscope (SEM) images well represent that particles of regolith simulants MGS-1 and LHS-1 have sharp angular shapes, whereas those of T-8 have a smoother shape (Figure 1).

Table 1. Properties of studied granular materials.

Granular Material	Mean Grain Density (g/cm^3)	Mean Diameter (μm)
MGS-1	3.23 [a]	90 [a]
LHS-1	3.19 [b]	90 [b]
T-8	2.78 [c]	120 [d]

[a] Exolith Lab. [b] Exolith Lab. [c] Ozaki et al. [41]. [d] Tabuchi et al. [42].

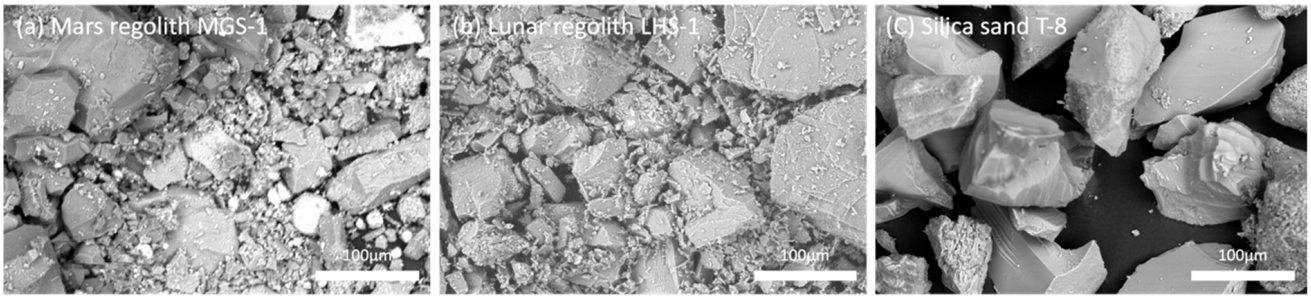


Figure 1. SEM images of studied granular materials. (**a**) Martian regolith simulant MGS-1, (**b**) Lunar regolith simulant LHS-1, and (**c**) Silica sand T-8. SEM images were acquired using JSM-IT700HR (JEOL, Ltd., Tokyo, Japan).

2.2. Experimental Setup

Our study aims to examine the wet hypothesis that high-salinity flow contributes to RSL formation processes through the most simple and generic lab experiments possible. In our experiments, we filled the given granular materials into a container with 87 mm height, 135 mm width, and 5 mm depth to prepare the given granular media where we flow testing liquids. The granular media was carefully prepared on a level platform, and the surface was flattened using an anti-static spatula. While lateral heterogeneity might exist locally across samples and among trials, the packing fraction of the given granular media fell within 33 ± 2%. The packing fraction well agrees with the actual data at the uppermost

10 cm column of lunar highland regolith [43–45], although the data are currently unavailable on the Martian surfaces. After filling, a polyvinyl chloride tube with an inner diameter of 6.0 mm was installed at the top of the granular media. Following Imamura et al. [46], we used a low-volumetric flow pump TP-1973R (AS ONE Corporation, Osaka, Japan) to control the continuous flow testing liquid on the granular media at a constant flow rate. As growth rates of actual RSL on Mars can reach 20 m per Martian day [13], this can be translated to a downslope growth rate of the flow trace of approximately 1.4 cm/min. Given this growth rate and optimal experimental condition for best recording the flow traces of pure water, we studied the flow rates of 1.8 g/min and 2.5 g/min for both high-salinity water (4.5 mol/kg $CaCl_2$ solution) and pure water while maintaining a room temperature of ~20 °C. To study the influences of inclination (θ) on downslope liquid flow (Figure 2), the container filled with the given granular material was fixed at inclinations of 17°, 9°, and 3°, adjusted by a digital inclinometer GLM500 Professional (Robert Bosch GmbH, Stuttgart, Germany). Given the Martian gravity is 1/3 of Earth's gravity, the inclinations of 17°, 9°, and 3° in our experimental conditions (Earth's gravity) can be translated to 61°, 28°, and 9° in Martian gravity, respectively, calculated from $gsin\theta$ where g is gravitational acceleration. Our downslope flow experiments require an environment that can produce very long-duration, continuous, and steady liquid flow. This inclination correction is the only method currently available to conduct our downslope flow experiments of the Martian gravity field other than in situ experiments on the Martian surface [42,47]. However, the inclination correction may not accurately represent the additional forces imposed on the actual liquid flow by friction and lateral stresses [47] on liquid-regolith and regolith-container surfaces, as infiltration and overall downslope velocity are still subject to the Earth's gravitational condition.

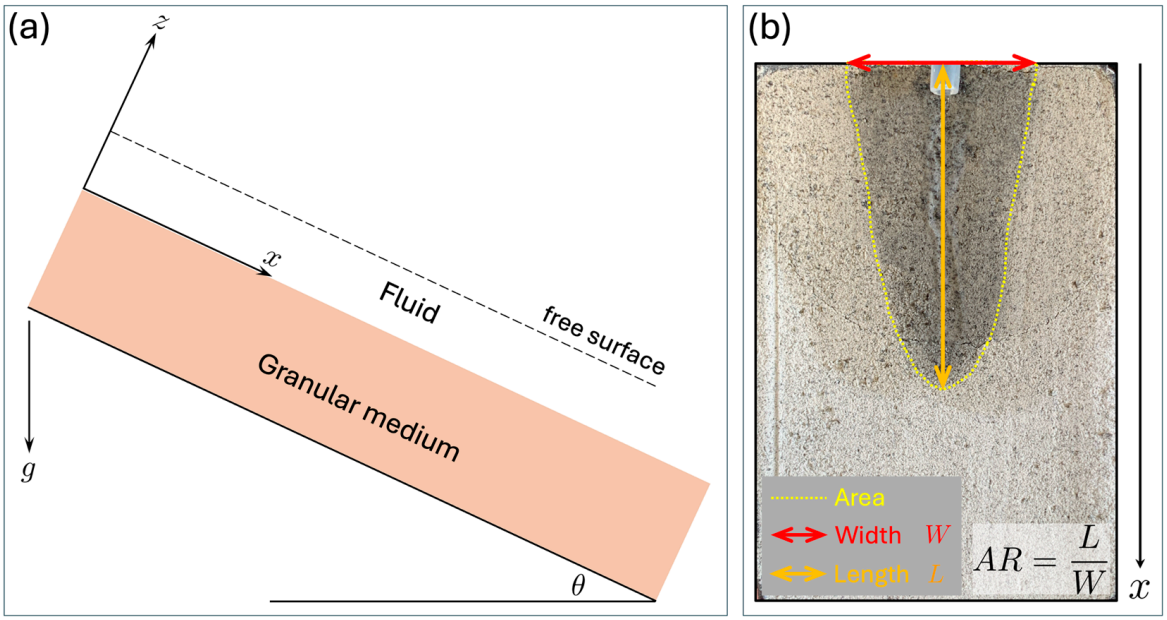


Figure 2. (**a**) Schematic illustration of our experiment with coordinates. (**b**) Definition of *AR* and areal extent of flow trace.

We acquired images of flow traces throughout the given downslope liquid flow experiment. The duration for flowing the given fluid was 60 s. After stopping the fluid flow, the granular media were dried in an oven at 40 °C for 24 h. While drying, the granular media-containing container was fixed at the given testing inclination in the dry oven. After drying, the same testing liquid was flowed again at the same flow rate. We systematically repeated these processes four times. The acquired flow trace images were analyzed using

Fiji/ImageJ version 1.54 [48,49]. The image analyses included geometry acquisitions and areal calculations of the given flow trace. From the image analyses, we also obtained the aspect ratio (AR) of the given flow trace defined by

$$AR(N) = L(N)/W(N), \quad (1)$$

where $L(N)$ and $W(N)$ are the maximum length and maximum width of the given flow trace at Nth liquid flow (N = 1, 2, 3, 4), respectively (Figure 2). We conducted three times for each flow experiment to assess the reproducibility in the obtained AR and areal extent of flow trace at the given experiment condition. All the results of AR and areal extents of the given flow trace are presented in $\mu \pm \sigma$, where μ and σ are the mean and one standard deviation of the given data (see Supplementary Materials).

3. Results

3.1. Flow Rates

In our experiment, we flowed a high-salinity liquid ($CaCl_2$(aq)) at two different flow rates, 1.8 g/min and 2.5 g/min. For example, Figure 3 shows the flow traces of the downslope high-salinity liquid ($CaCl_2$(aq)) flow in the MGS-1, LHS-1, and T-8 granular column at a constant flow rate of 2.5 g/min and inclination of 17°. The flow trace on the surface of the MGS-1 granular media was first in a relatively tonguelike shape at $N = 1$ and increased length in slope direction relative to width at higher Nth of flow (Figure 3). AR significantly rose from $AR(1)$ = 1.41 ± 0.09 at $N = 1$ to $AR(4)$ = 3.33 ± 0.20 at $N = 4$, respectively (Figure 4), resulting in a 3.3 times increase. The energy dispersive X-ray spectrometer (EDS) analysis of the granular materials sampled on their uppermost column after the liquid flow showed an increase in Ca and Cl. The results represent $CaCl_2$ deposition within the MGS-1 granular media due to the high-salinity liquid ($CaCl_2$(aq)) flow (Figure 5). The LHS-1 granular column at the same flow and slope condition also showed a growth of flow trace in slope direction and an increase in AR with higher Nth of flow (Figure 4), resulting in $AR(1)$ = 0.92 ± 0.12 at $N = 1$ to $AR(4)$ = 2.07 ± 0.18 at $N = 4$, respectively. In contrast, the T-8 granular column showed a distinctive flow trace, characterized by nearly no growth of flow trace in slope direction (Figure 3) with very few changes in AR (Figure 4).

Likewise, the MGS-1 and LHS-1 granular columns at a flow rate of 1.8 g/min also showed a growth of flow trace in slope direction (Figure 6) and an increase in AR with higher Nth of flow (Figure 4). For example, the AR of flow trace in the MGS-1 granular media increased from $AR(1)$ = 0.91 ± 0.11 at $N = 1$ to $AR(4)$ = 2.68 ± 0.03 at $N = 4$, respectively (Figure 4), resulting in a 2.9 times increase. The increase rate in $AR(N)$ at a flow rate of 1.8 g/min was thus lower than that at 2.5 g/min due to the lower flow rate. On the other hand, the T-8 granular column at 1.8 g/min had very slight growth in flow trace with asymmetric, representing the unchanged AR, as observed when the flow rate was 2.5 g/min (Figure 4).

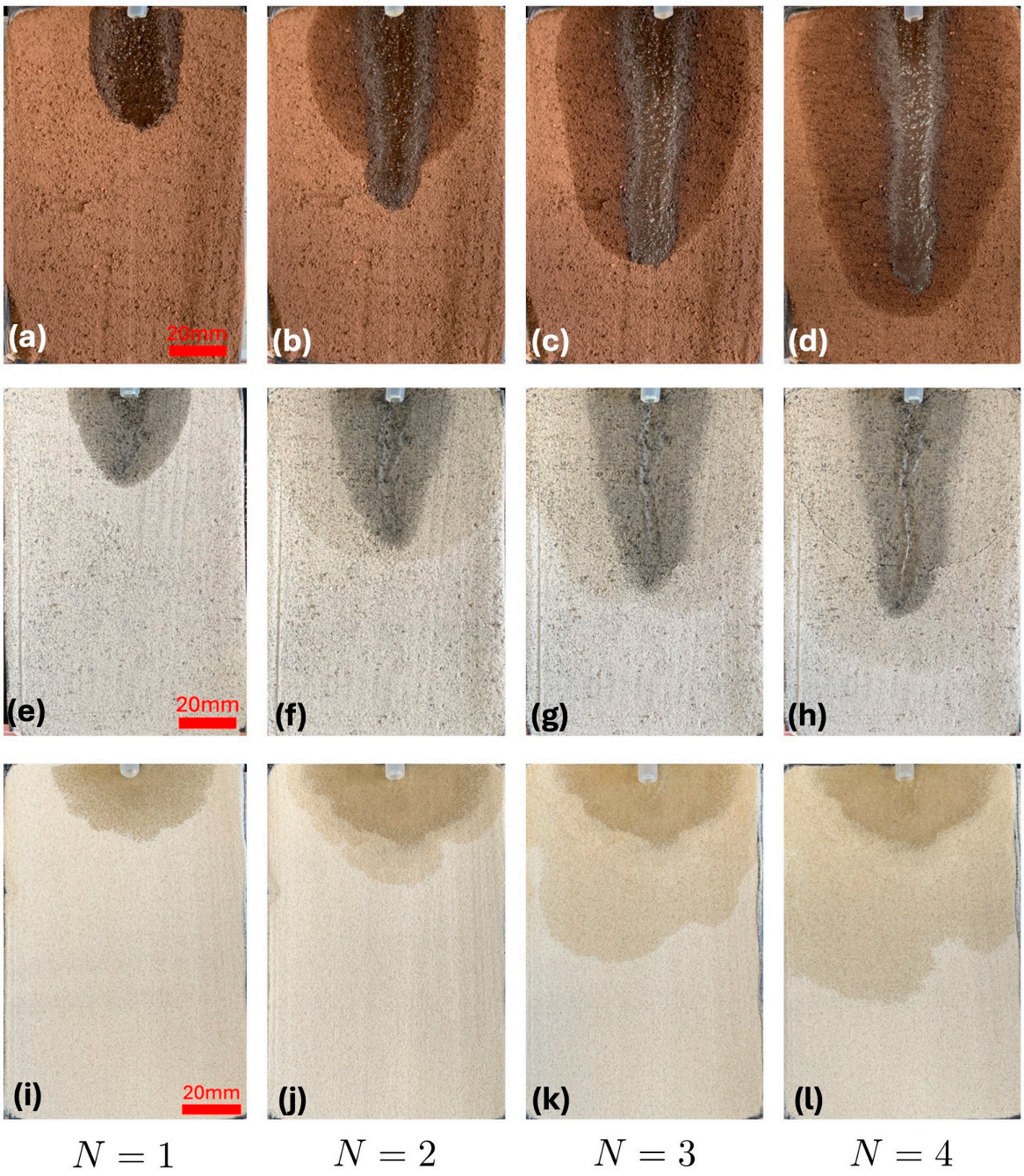


Figure 3. Flow trace of downslope fluid flow in the MGS-1 granular column with 2.5 g/min of $CaCl_2$(aq) flow on a 17° slope at (**a**) $N = 1$, (**b**) $N = 2$, (**c**) $N = 3$, and (**d**) $N = 4$. Flow trace of downslope fluid flow in the LHS-1 granular column with 2.5 g/min of $CaCl_2$(aq) flow on a 17° slope at (**e**) $N = 1$, (**f**) $N = 2$, (**g**) $N = 3$, and (**h**) $N = 4$. Flow trace of downslope fluid flow in the T-8 granular column with 2.5 g/min of $CaCl_2$(aq) flow on a 17° slope at (**i**) $N = 1$, (**j**) $N = 2$, (**k**) $N = 3$, and (**l**) $N = 4$.

As expected from the results in increasing AR, the areal extent of flow trace almost linearly increased with higher Nth of flow in all the studied granular materials (Figure 7). The T-8 had the least areal extent among the studied granular materials. MGS-1 and LHS-1 showed a tendency to have larger areas than T-8. At first flow ($N = 1$) with 2.5 g/min, the areal extents were 1317 ± 3 mm^2, 1338 ± 178 mm^2, and 1437 ± 335 mm^2 in the MGS-1, LHS-1, and T-8 granular media, respectively. At the fourth flow ($N = 4$) with 2.5 g/min, the areal extents were 2201 ± 6 mm^2, 2690 ± 31 mm^2, and 1976 ± 415 mm^2 in the MGS-

1, LHS-1, and T-8 granular media, respectively, resulting in an averaged difference of 714 mm^2 between MGS-1 and T-8. All the granular materials formed more extensive flow traces at a flow rate of 2.5 g/min than at 1.8 g/min.

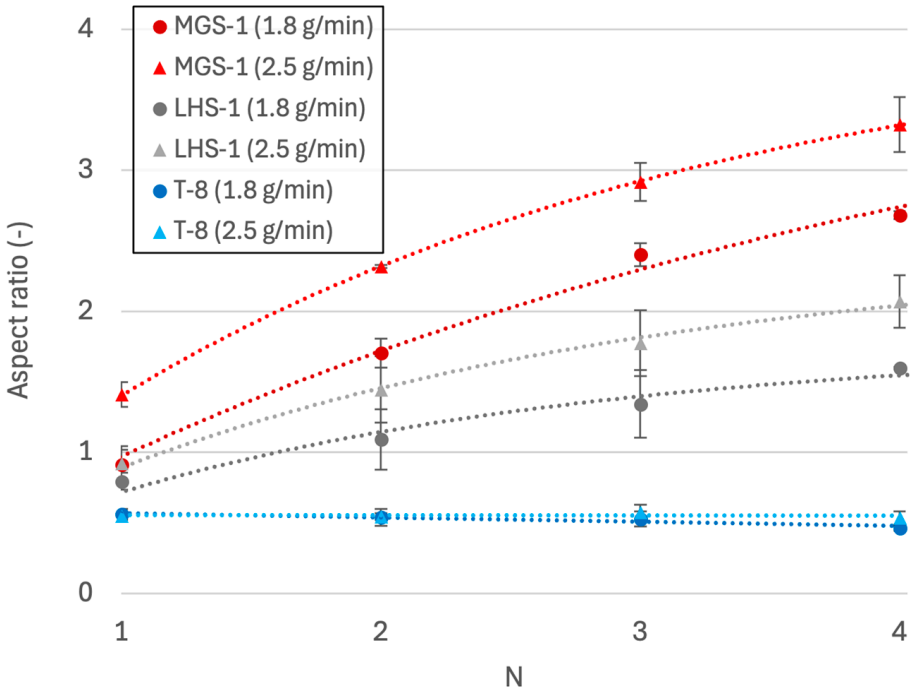


Figure 4. Changes in aspect ratio $AR(N)$ of $CaCl_2$(aq) flow trace in the MGS-1, LHS-1, and T-8 granular media on a 17° slope at flow rates of 1.8 g/min and 2.5 g/min.

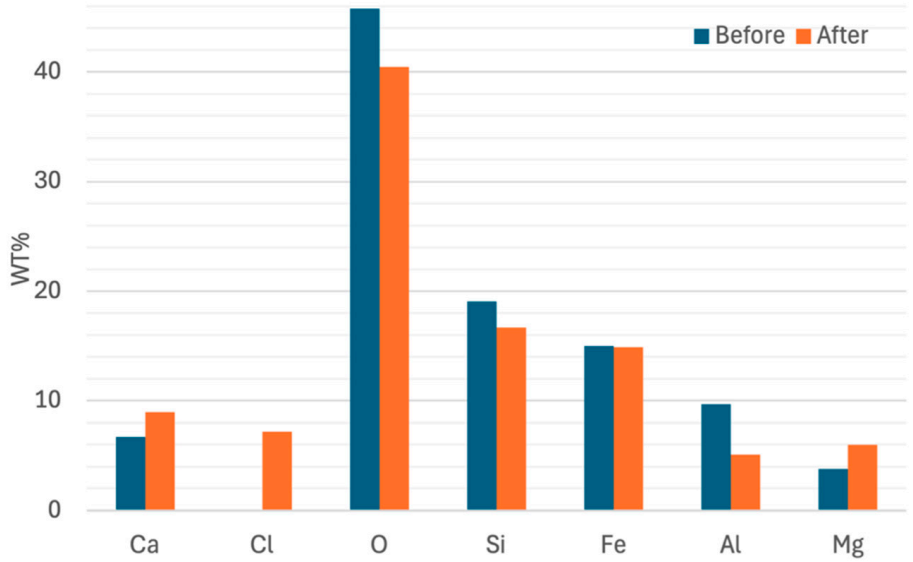


Figure 5. Changes in chemical compositions in the MGS-1 granular column before and after the high-salinity fluid flow ($N = 1$) identified by EDS analysis. The EDS analysis was performed using JSM-IT700HR (JEOL, Ltd., Tokyo, Japan).

3.2. Fluids

In our experiment, we examined the influence of high salinity on downslope liquid flow on the studied granular media by changing the two fluids: high-salinity water $CaCl_2$(aq) (4.5 mol/kg $CaCl_2$ solution) and pure water (H_2O). For example, Figure 8 shows the flow traces of the downslope H_2O flow in the MGS-1, LHS-1, and T-8 granular column at a constant flow rate of 1.8 g/min and inclination of 17°. The flow traces of H_2O flow

were different from those of high-salinity $CaCl_2$(aq) flow. The flow traces of H_2O flow did not grow significantly with higher Nth of flow (Figure 8). Their AR did not change throughout the experiment in all the granular media (Figure 9). The results revealed significant differences between the flow traces of high-salinity $CaCl_2$(aq) and H_2O flows in the MGS-1 and LHS-1 granular column. However, it should be emphasized that the choice of liquid did not alter AR in the T-8 granular column.

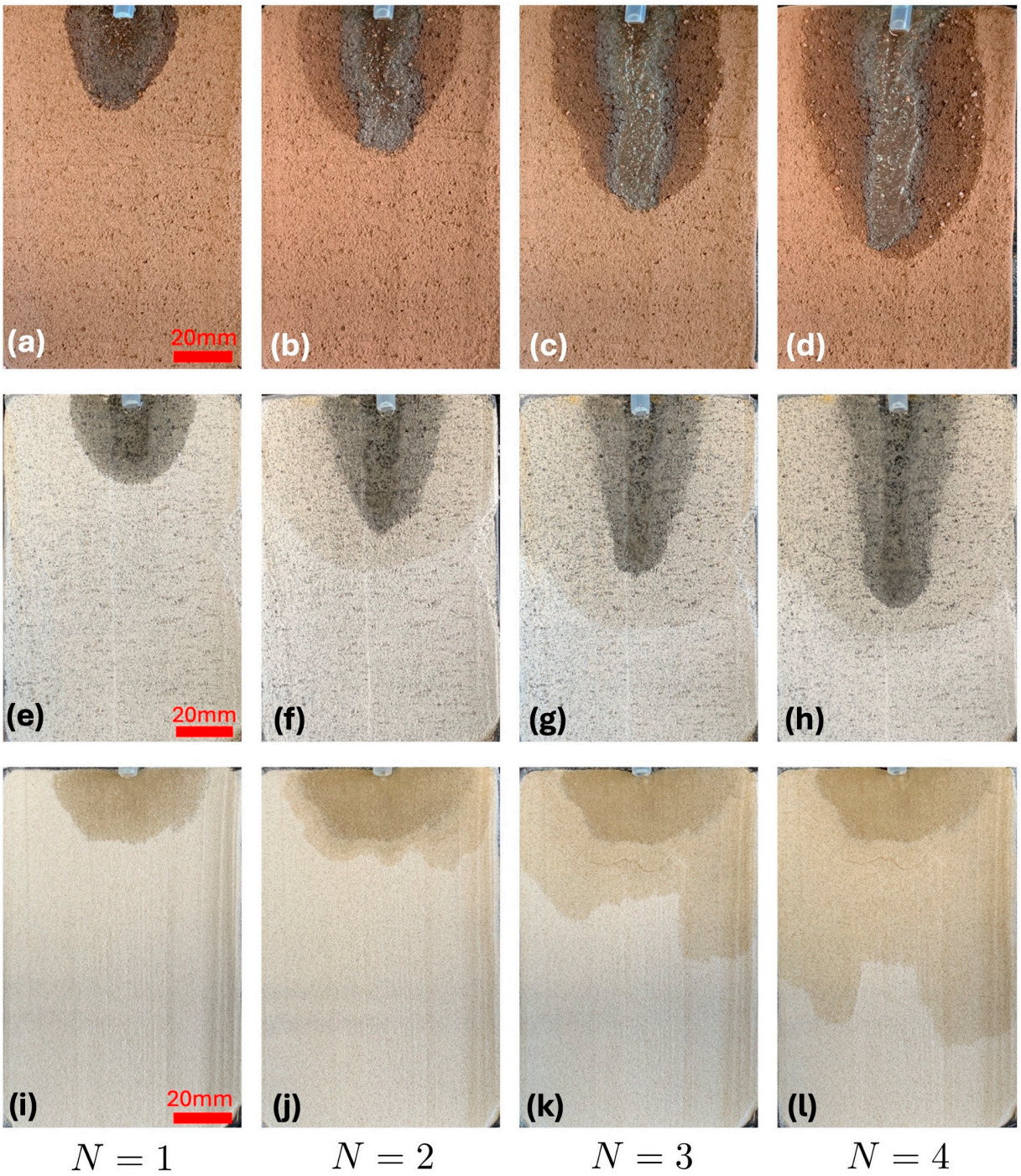


Figure 6. Flow trace of downslope fluid flow in the MGS-1 granular column with 1.8 g/min of $CaCl_2$(aq) flow on a 17° slope at (**a**) $N = 1$, (**b**) $N = 2$, (**c**) $N = 3$, and (**d**) $N = 4$. Flow trace of downslope fluid flow in the LHS-1 granular column with 1.8 g/min of $CaCl_2$(aq) flow on a 17° slope at (**e**) $N = 1$, (**f**) $N = 2$, (**g**) $N = 3$, and (**h**) $N = 4$. Flow trace of downslope fluid flow in the T-8 granular column with 1.8 g/min of $CaCl_2$(aq) flow on a 17° slope at (**i**) $N = 1$, (**j**) $N = 2$, (**k**) $N = 3$, and (**l**) $N = 4$.

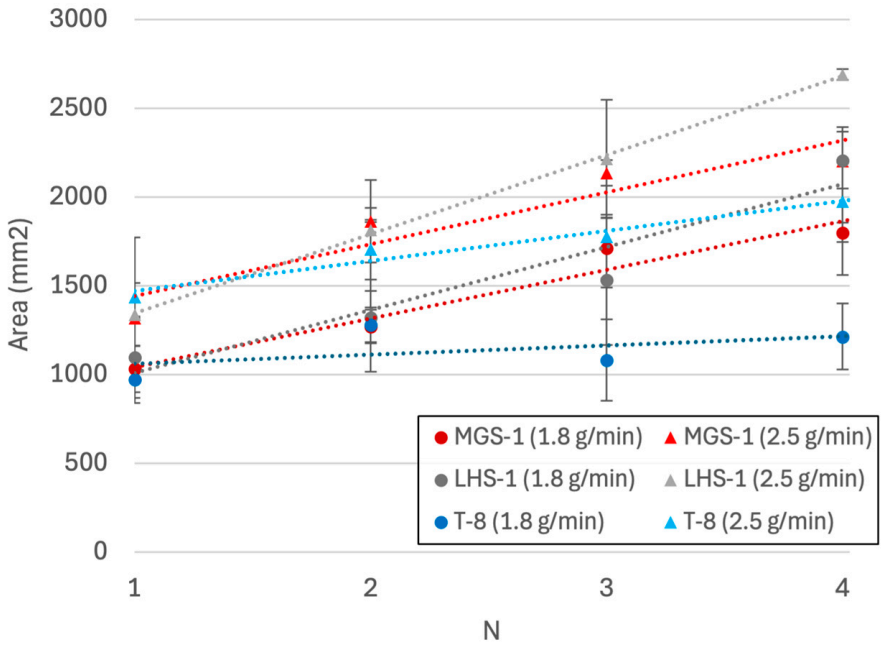


Figure 7. Changes in areal extents of $CaCl_2$(aq) flow trace in the MGS-1, LHS-1, and T-8 granular media on a 17° slope at flow rates of 1.8 g/min and 2.5 g/min.

3.3. Inclinations

In addition to flowing fluid and its flow rate, we studied the influence of inclination (slope) on downslope liquid flow on the studied granular media by changing the three inclinations 17° (equivalent to 61° in Martian gravity), 9° (28°), and 3° (9°). For instance, the results showed that the aspect ratios of $CaCl_2$(aq) flow trace at 2.5 g/min in the MGS-1 granular media (Figure 10a) were $(AR(3), AR(4))$ = $(1.73 \pm 0.08, 1.70 \pm 0.20)$ and $(AR(3), AR(4))$ = $(2.76 \pm 0.46, 3.02 \pm 0.47)$ at inclinations of 3° and 9°, respectively, lower than those at 17° inclination resulting $(AR(3), AR(4))$ = $(2.92 \pm 0.13, 3.33 \pm 0.20)$. The areal extent of $CaCl_2$(aq) flow trace in the given Nth flow at 2.5 g/min in the MGS-1 granular media was also generally lower when the inclination was lower (Figure 10b). Likewise, the aspect ratios of $CaCl_2$(aq) flow trace at 2.5 g/min in the LHS-1 granular media (Figure 11a) were $(AR(3), AR(4))$ = $(1.15 \pm 0.22, 1.36 \pm 0.31)$, and $(AR(3), AR(4))$ = $(1.70 \pm 0.14, 1.94 \pm 0.17)$ at inclinations of 3° and 9°, respectively, lower than those at 17° inclination resulting $(AR(3), AR(4))$ = $(1.77 \pm 0.23, 2.07 \pm 0.18)$. The areal extent of $CaCl_2$(aq) flow trace in the given Nth flow at 2.5 g/min in the LHS-1 granular media was also generally lower when the inclination was lower, although the difference was less significant than that in the MGS-1 granular media (Figure 11b). In contrast, the flow trace of $CaCl_2$(aq) flow in the given Nth flow at 2.5 g/min in the T-8 granular media showed the aspect ratio $AR(N)$ at the Nth flow in the T-8 granular media was unchanged at all the studied inclinations (Figure 12a) with homothetic growth (Figure 12b).

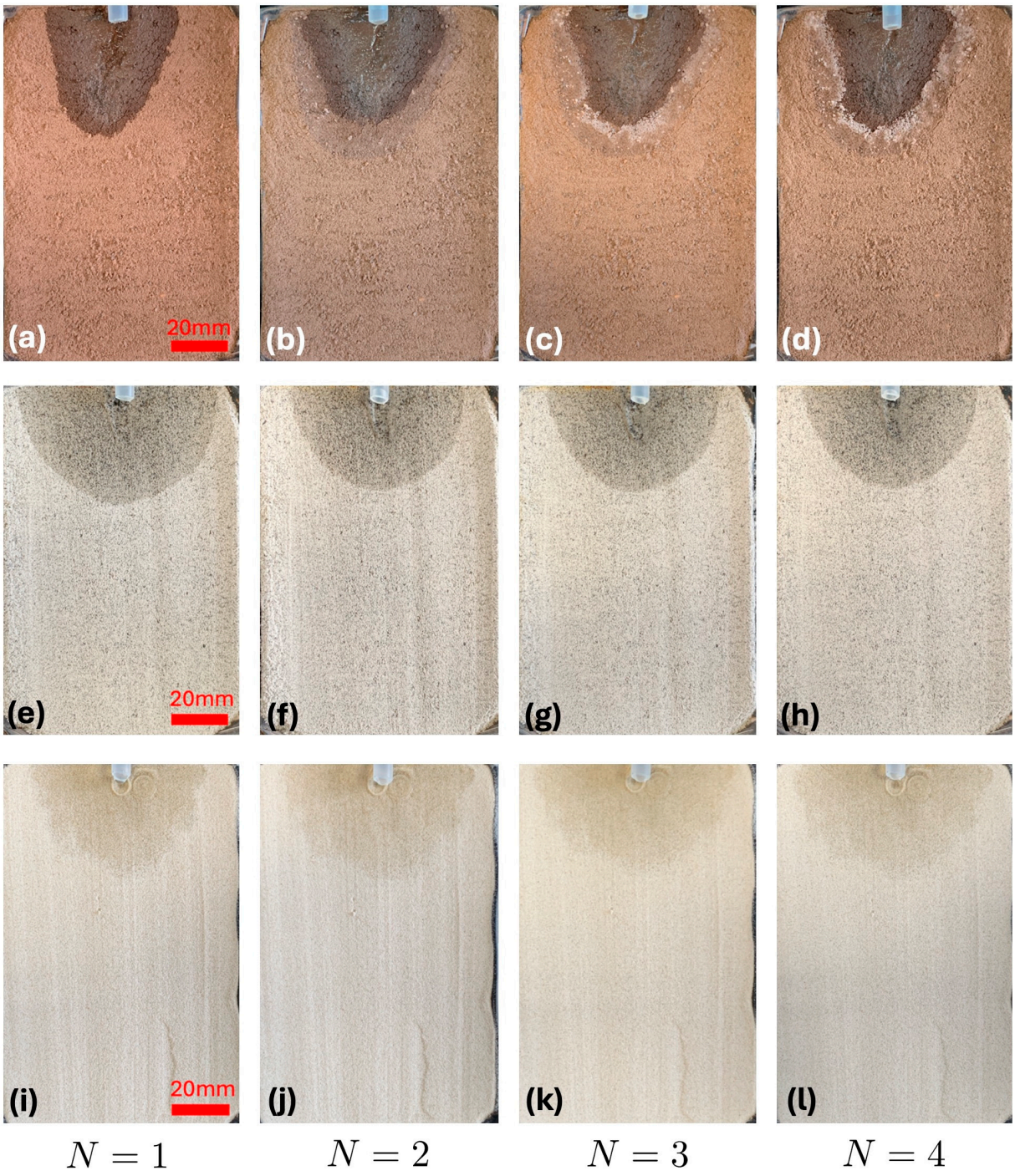


Figure 8. Flow trace of downslope fluid flow in the MGS-1 granular column with 1.8 g/min of water flow on a 17° slope at (**a**) $N = 1$, (**b**) $N = 2$, (**c**) $N = 3$, and (**d**) $N = 4$. Flow trace of downslope fluid flow in the LHS-1 granular column with 1.8 g/min of water flow on a 17° slope at (**e**) $N = 1$, (**f**) $N = 2$, (**g**) $N = 3$, and (**h**) $N = 4$. Flow trace of downslope fluid flow in the T-8 granular column with 1.8 g/min of water flow on a 17° slope at (**i**) $N = 1$, (**j**) $N = 2$, (**k**) $N = 3$, and (**l**) $N = 4$.

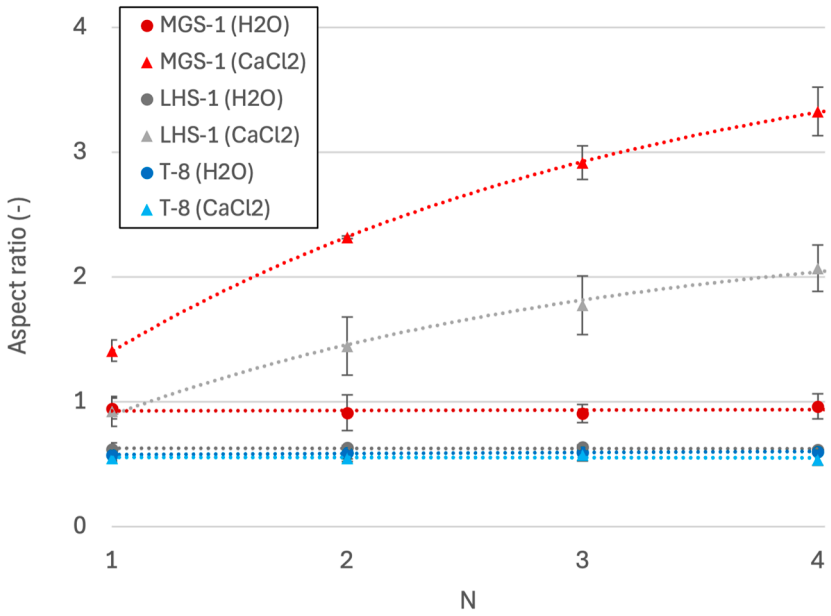


Figure 9. Changes in aspect ratio $AR(N)$ in the MGS-1, LHS-1, and T-8 granular media on a 17° slope with different fluids, $CaCl_2$(aq) and pure water (H_2O).

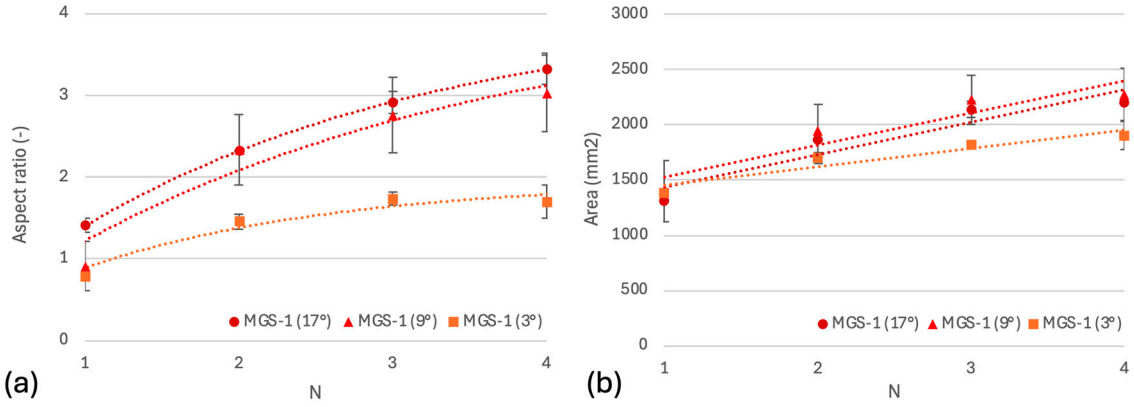


Figure 10. (**a**) Changes in aspect ratio $AR(N)$ of $CaCl_2$(aq) flow trace at 2.5 g/min in the MGS-1 granular media on 17°, 9°, and 3° slopes. (**b**) Changes in areal extents of $CaCl_2$(aq) flow trace at 2.5 g/min in the MGS-1 granular media on 17°, 9°, and 3° slopes.

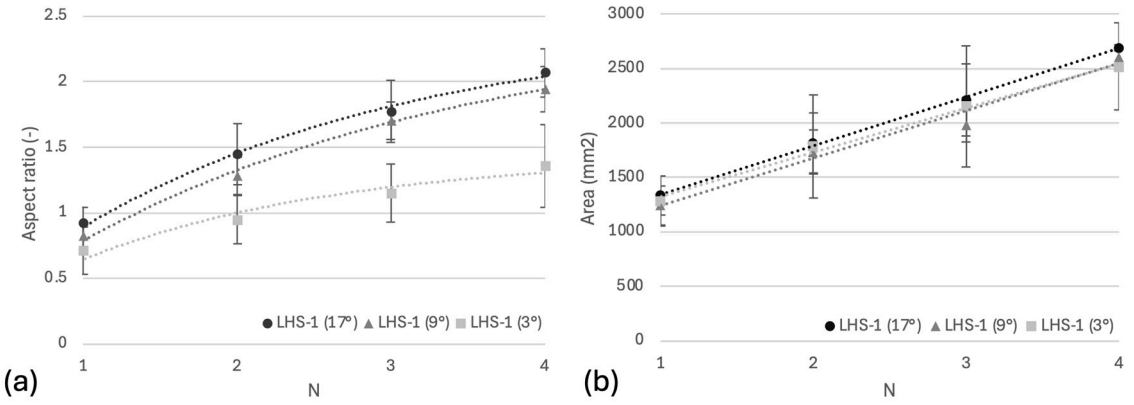


Figure 11. (**a**) Changes in aspect ratio $AR(N)$ of $CaCl_2$(aq) flow trace at 2.5 g/min in the LHS-1 granular media on 17°, 9°, and 3° slopes. (**b**) Changes in areal extents of $CaCl_2$(aq) flow trace at 2.5 g/min in the LHS-1 granular media on 17°, 9°, and 3° slopes.

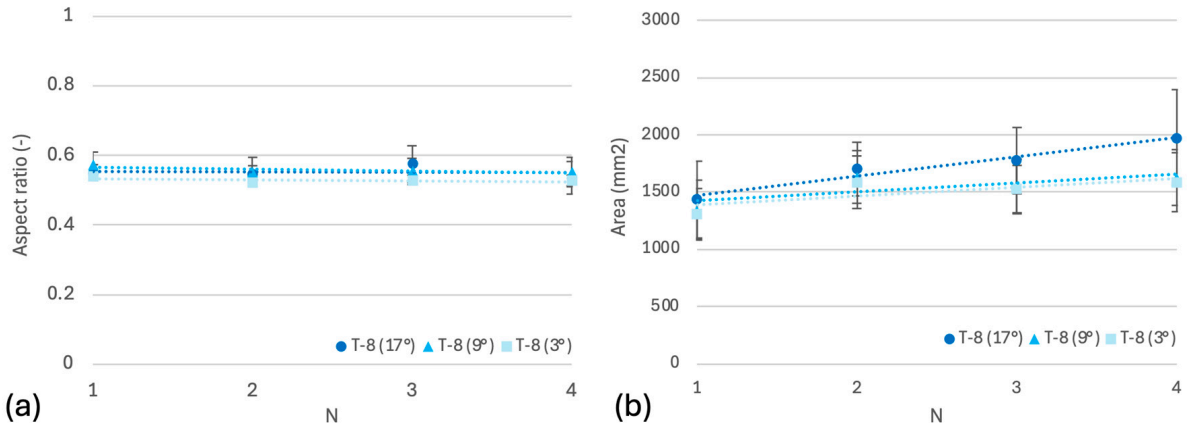


Figure 12. (**a**) Changes in aspect ratio $AR(N)$ of $CaCl_2$(aq) flow trace at 2.5 g/min in the T-8 granular media on 17°, 9°, and 3° slopes. (**b**) Changes in areal extents of $CaCl_2$(aq) flow trace at 2.5 g/min in the T-8 granular media on 17°, 9°, and 3° slopes.

4. Discussion

4.1. Effect of Materials

4.1.1. Permeability of Studied Granular Materials

We tested three different granular materials (i.e., Martian regolith simulant MGS-1, lunar regolith simulant LHS-1, and terrestrial fine silica sand T-8) and studied the downslope high-salinity fluid flow on the given granular media in our experiment. The experiment results revealed a significant difference in ARs of flow trace due to high-salinity fluid flow among the studied granular materials. Many previous studies reported the physical and geomechanical properties of the granular materials [38–40,42,50,51]. For example, one of the previous studies using the same regolith simulants reported that regolith materials show significantly lower permeability than terrestrial fine sand due to their complex particle shape [42]. The low permeability thus relates to our findings that the downslope high-salinity fluid resulted in predominating surface flow, leading to large ARs in flow trace (Figures 4, 10 and 11). In contrast, the terrestrial fine sand encouraged the high-salinity fluid to have a more permeable flow than surface flow due to its moderate permeability and smooth particle shape. Additionally, the high-salinity fluid flow spreads not only in the downslope (length) direction but also in the lateral (width) direction, leading to more circular flow traces and low ARs (Figures 4 and 12). Thus, these findings suggest that the regolith favors generating long-distance flow trace (i.e., RSL formation) more than terrestrial fine sand.

Nevertheless, our results further revealed that ARs of flow trace in the Martian regolith simulant media were higher than the lunar regolith simulant (Figures 4, 10 and 11). The permeability is commonly expressed by the Kozeny–Carman equation:

$$k = \frac{(1-\eta)^3}{B\eta^2\tau^2}\overline{D}^2, \quad (2)$$

where k is permeability, η is packing fraction, B and τ are the shape factor and tortuosity of the flow path, respectively, and $\overline{D}$ is the mean diameter of particles [52]. Here, the mean diameter of particles (Table 1) and the shape parameter of particles (e.g., particle aspect ratio, elongation, sphericity, perimeter) [40] related to the shape factor are nearly identical between Martian and lunar regolith simulants (Table 1). Also, the packing fraction was well controlled not to vary among the studied granular media in our experiments (see Section 2). However, particle size distributions show that the 10% and 50% curvature coefficients (D_{10} and D_{50}) of the MGS-1 sample are lower than those of the LHS-1 sample [40], indicating

that the Martian regolith simulants contain more small particles than the lunar regolith simulants. This may help higher tortuosity and result in lower permeability in the Martian regolith simulant than the lunar regolith simulant, allowing the representation of larger aspect ratios in the Martian regolith simulant than the lunar regolith simulant.

4.1.2. Beavers–Joseph (BJ) Boundary Condition

Below, we aim to discuss the boundary between the two media (i.e., flowing high-salinity liquid and granular materials) by modeling the flow of the liquid over the porous medium. Assuming that the flow within the granular medium satisfies Darcy's law in our experiments, the interface boundary condition, related to interfacial slip velocity, Darcy's velocity, and permeability of the porous medium, can be expressed in a general form by [53]:

$$\frac{\partial u_i}{\partial z} + J\frac{\partial u_3}{\partial x_i} = \frac{\alpha_{BJ}}{\sqrt{k}}(u_i - u_i^m)(i = 1,\ 2), \tag{3}$$

where $\boldsymbol{u} = (u_1, u_2, u_3)$ is the fluid velocity, $\boldsymbol{u^m} = \left(u_1^m, u_2^m, u_3^m\right)$ is the Darcy velocity inside the porous medium, z is the direction perpendicular to the interface (Figure 2), and α_{BJ} is the Beavers–Joseph (BJ) coefficient. By taking $J = 0$, Equation (3) can be represented as the Beavers and Joseph's equation [54]:

$$\frac{\partial u}{\partial z} = \frac{\alpha_{BJ}}{\sqrt{k}}(u - u^m), \tag{4}$$

where u is the fluid velocity and u^m is the Darcy velocity inside the porous medium. Here, the Darcy velocity u^m is estimated by:

$$u^m = \frac{k}{\mu}\frac{dp}{dx}, \tag{5}$$

where μ is the fluid viscosity and p is pressure. From the reported permeability for regolith simulants [42], the Darcy velocity u_m was calculated to be on the order of magnitudes of 10^{-12}–10^{-11} m/s. From the observed averaged fluid velocity, the Darcy velocity satisfies $u^m \ll u$ in most of the z ranges, allowing us to neglect the Darcy flow [55] and approximate Equation (4) to:

$$\frac{du}{dz} \sim \frac{\alpha_{BJ}}{\sqrt{k}}u. \tag{6}$$

From Equation (6), we could obtain the BJ coefficient of the given granular materials using the estimated mean flow velocity from the length of flow trace at Nth flow (Table 2) by assuming the thickness of the thin flow layer identical between granular materials. The BJ coefficient is generally related to various factors, including interfacial location, microstructure surfaces, fluid properties, and flow conditions [27,56]. For example, the BJ coefficient of the granular material is larger when the mean diameter is larger given the identical particle shape [56]. Our estimations showed that the BJ coefficients differed by the studied granular materials, representing $\alpha_{BJ}^{MGS-1} < \alpha_{BJ}^{LHS-1} < \alpha_{BJ}^{T-8}$ (Table 2), where α_{BJ}^{MGS-1}, α_{BJ}^{LHS-1}, and α_{BJ}^{T-8} indicate BJ coefficients of MGS-1, LHS-1, and T-8, respectively. This indicates that our results showing the largest ARs in the Martian regolith simulants are due to their low BJ coefficient, probably explained by their distinctive microstructure surfaces and interfacial location.

Table 2. Ratios of BJ coefficients obtained from $CaCl_2$(aq) flow trace with 2.5 g/min of water flow on 17° slope at Nth flow.

N	$\alpha_{BJ}^{LHS-1}/\alpha_{BJ}^{T-8}$	$\alpha_{BJ}^{MGS-1}/\alpha_{BJ}^{T-8}$	$\alpha_{BJ}^{MGS\text{-}1}/\alpha_{BJ}^{LHS\text{-}1}$
1	0.464	0.448	0.966
2	0.433	0.415	0.958
3	0.422	0.403	0.956
4	0.405	0.394	0.971

4.1.3. Type of Fluids

In our experiment, we tested two different liquids (i.e., pure water and high-salinity water with 4.5 mol/kg $CaCl_2$ solution) and studied the downslope liquid flow on several different granular media. The experiment results revealed a significant difference in ARs of flow trace between the two different fluids. The flow trace with H_2O flow in all the granular media showed lower ARs (Figure 9). This result is also related to the fluid viscosity because the viscosity of our $CaCl_2$(aq) is approximately 4 times higher than that of pure water [57]. The high viscosity decreases the Darcy velocity, resulting in surface flow being more dominant than permeable flow in the $CaCl_2$(aq) flow. Our results further showed that the increase in ARs of $CaCl_2$(aq) flow traces on the regolith simulant media was pronounced in the second ($N = 2$) and/or third ($N = 3$) flow (Figures 4 and 9–11), although it was not observed in water flow traces. This may be because the precipitation of solid $CaCl_2$ within the granular media due to drying after the first ($N = 1$) flow (Figure 5) decreased the permeability, further encouraging the surface flow on the regolith simulant media surface.

4.2. Implications for Actual RSL on the Martian Surface

Our experiment results showed that the aspect ratio $AR(N)$ of $CaCl_2$(aq) flow trace in the regolith simulant granular media increases with higher N while it approaches asymptotically to a certain value (e.g., Figure 4). We thus assumed a simple relationship between the aspect ratio $AR(N)$ and N expressed by

$$AR(N) = a\left(1 - b^N\right), \tag{7}$$

where a and b are constants. We derived the constant (horizontal asymptote) a in the given experiment condition by a nonlinear regression analysis because it represents the AR of the flow trace approached with higher Nth flow. The constant a in the $CaCl_2$(aq) flow at with 2.5 g/min on the Martian regolith simulant media was 1.96 ± 0.19, 4.16 ± 1.08, and 4.07 ± 0.02 at inclinations of 3° (equivalent to 9° in Martian gravity), 9° (28°), and 17° (61°), respectively. These values should agree with the AR of RSL on the Martian surfaces if the downslope high-salinity liquid flow forms actual RSL.

The actual RSL features are generally recognized on slopes greater than 25° on Martian surfaces [20,25,58]. We compiled the data of geomorphological properties available in the Palikir, Horowitz, and Raga Craters [25,58] on Mars to understand the AR and formed slope of actual RSL on Mars (Figure 13). The compilation showed that the RSL formations are primarily present on Martian slopes of 25–50°, with their broad range of ARs of 1.4–90, 2.0–180, and 0.9–400 in the Palikir, Horowitz, and Raga Craters, respectively (Figure 13). Our result of a = 4.16 ± 1.08 in the $CaCl_2$(aq) flow at 2.5 g/min on Martian-equivalent gravity of 28°, calculated from Equation (7), fell within the ARs of actual RSL on Mars (Figure 13).

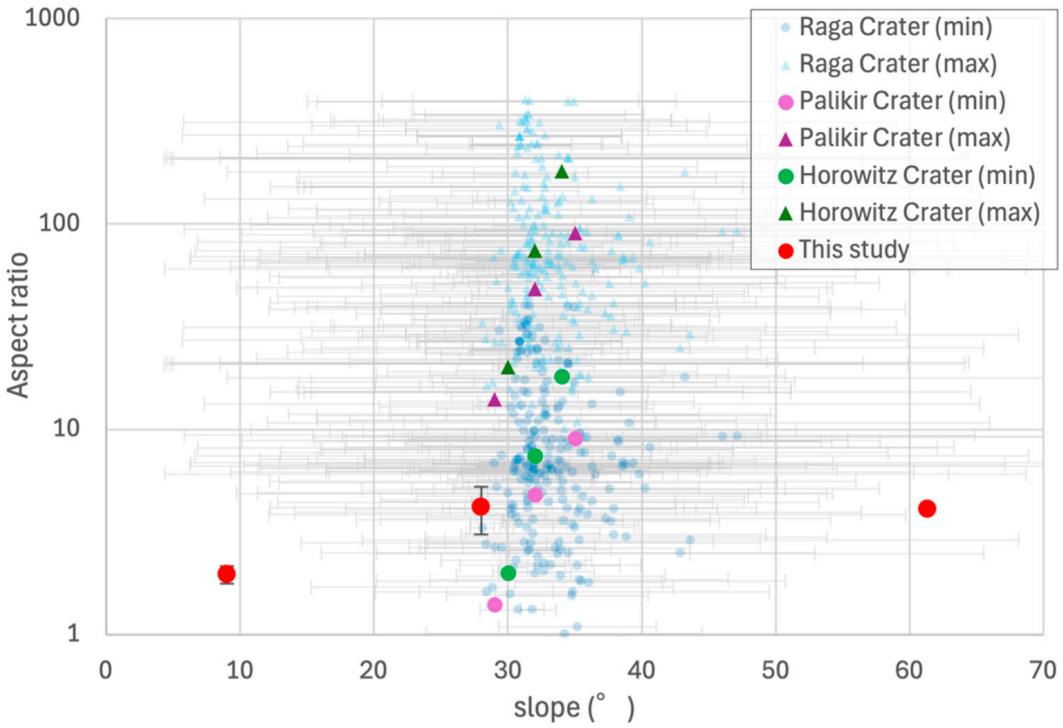


Figure 13. Aspect ratios of $CaCl_2$(aq) flow trace at 2.5 g/min in the Martian regolith simulants from our study (red), and aspect ratios of RSLs identified in the Raga crater [58] (light blue), Palikir crater [25] (purple), and Horowitz crater [25] (green). Gray error bars show the ranges of the Martian slope forming the respective RSL available from published data [25,58]. Note that the aspect ratio of the respective RSL was provided with its minimum and maximum value due to the variable width and length available at the respective RSL.

While our results of $a = 4.16 \pm 1.08$ in the $CaCl_2$(aq) flow at 2.5 g/min on Martian-equivalent gravity of 28° fell within the ARs of actual RSL on Mars, many of actual RSL observed on Mars yield higher ARs than 4.16 ± 1.08 (Figure 13). This deviation may suggest that actual RSL evolves through many more multiple cycles of flows and drying, while the constant a is obtained by projecting the AR at a sufficiently high number of cycles, as presented in Equation (7). If acquiring the results at higher N than our study alters the constant a, while our experiment observes the stability at $N = 4$, it can indicate the persistence or recurrence of actual RSL. Our experiment demonstrated the monotonic increase in AR with higher N, suggesting that RSL with higher ARs experiences more cycles of high-salinity flows and drying. Furthermore, our experiment showed that the AR of the flow trace increases with a higher flow rate of high-salinity flow (Figure 4). This suggests that variable ARs of actual RSL at the given slope can be partly explained by variable flow rates of high-salinity flow, as well as salinity (i.e., viscosity) of flow. If this hypothesis is correct, ARs of RSL can suggest the temporal dynamics of brine hydration and salt formation and the magnitude and frequency of daily and seasonal cycles at the regions forming the given RSL. Anyhow, our experimental study supports the hypothesis that RSL formation is due to high-salinity liquid flow on slopes, although further studies are necessary to better understand the actual RSL identified on Mars.

5. Conclusions

This paper studied high-salinity downslope liquid flow on the regolith simulant media to examine the hypothesis that brine liquid forms Recurring Slope Lineae (RSL) on Martian surfaces. We experimentally reproduced RSL-like features on Martian regolith using high-salinity liquid ($CaCl_2$(aq)) and regolith simulants. We obtained aspect ratios

(ARs) of resulting flow traces, the ratios of length to width of flow traces, to understand how ARs vary with the underlying granular material column (Martian regolith simulant MGS-1, lunar regolith simulant LHS-1, and terrestrial fine sand T-8), liquid (pure water and high-salinity $CaCl_2$(aq)) and its flow rate (2.5 g/min and 1.8 g/min), and inclination (Martian equivalent 9°, 28°, and 61°). The key findings of our study are below:

- Although ARs of the fluid trace of pure water (H_2O) were lower than 1.0, those of the high-salinity fluid trace reached greater than 4.0, indicating that pure water is incapable of forming RSL-like features.
- ARs of high-salinity fluid ($CaCl_2$(aq)) trace on Martian regolith simulants are among the largest in the studied granular materials, including other regolith simulants and terrestrial fine sands.
- ARs of high-salinity fluid ($CaCl_2$(aq)) trace well agree with the observations of actual RSL identified in Raga, Palikir, and Horowitz craters on Martian slopes.
- Martian regolith simulant represents the lowest permeability and Beavers–Joseph coefficient among the studied granular materials, highlighting the distinctive microstructure surfaces and interfacial location of Martian regolith. This encourages surface flow on the Martian regolith surface rather than Darcy flow within the regolith column, leading to a narrow and long-distance feature with high ARs of RSL identified on the Martian surface.

Although further studies are necessary to investigate other possible physical processes (e.g., "slope failure hypothesis" and dry granular flows), our findings provide support for the wet hypothesis that high-salinity flow contributes to RSL formation processes. Our study has profound implications for our understanding of Martian surface features and the potential for salts on Mars.

Supplementary Materials: The following supporting information can be downloaded at: https://www.mdpi.com/article/10.3390/fluids10070183/s1.

Author Contributions: Conceptualization, Y.T. and A.K.; data curation, Y.T. and A.K.; formal analysis, Y.T. and A.K.; funding acquisition, A.K.; investigation, Y.T., A.K., and T.T.; methodology, Y.T. and A.K.; project administration, A.K.; resources, A.K.; software, Y.T. and A.K.; supervision, A.K. and Y.Y.; validation, Y.T. and A.K.; visualization, Y.T. and A.K.; writing—original draft, Y.T. and A.K.; writing—review and edit, A.K. and T.T. All authors have read and agreed to the published version of the manuscript.

Funding: This work was supported by JSPS KAKENHI Grant-in-Aid for Early-Career Scientists JP23K13698.

Data Availability Statement: The datasets presented in this study are available in Supplementary Materials.

Conflicts of Interest: The authors declare that they have no known competing financial interests or personal relationships that could have appeared to influence the work reported in this paper.

References

1. Mangold, N.; Kite, E.S.; Kleinhans, M.G.; Newsom, H.; Ansan, V.; Hauber, E.; Kraal, E.; Quantin, C.; Tanaka, K. The origin and timing of fluvial activity at Eberswalde crater, Mars. *Icarus* **2012**, *220*, 530–551. [CrossRef]
2. de Quay, G.S.; Kite, E.S.; Mayer, D.P. Prolonged Fluvial Activity From Channel-Fan Systems on Mars. *J. Geophys. Res. Planets* **2019**, *124*, 3119–3139. [CrossRef]
3. Galofre, A.G.; Bahia, R.S.; Jellinek, A.M.; Whipple, K.X.; Gallo, R. Did Martian valley networks substantially modify the landscape? *Earth Planet. Sci. Lett.* **2020**, *547*, 116482. [CrossRef]
4. Mangold, N.; Gupta, S.; Gasnault, O.; Dromart, G.; Tarnas, J.D.; Sholes, S.F.; Horgan, B.; Quantin-Nataf, C.; Brown, A.J.; Le Mouélic, S.; et al. Perseverance rover reveals an ancient delta-lake system and flood deposits at Jezero crater, Mars. *Science* **2021**, *374*, 711–717. [CrossRef]

5. Bibring, J.-P.; Langevin, Y.; Poulet, F.; Gendrin, A.; Gondet, B.; Berthé, M.; Soufflot, A.; Drossart, P.; Combes, M.; Bellucci, G.; et al. Perennial water ice identified in the south polar cap of Mars. *Nature* **2004**, *428*, 627–630. [CrossRef]
6. Plaut, J.J.; Picardi, G.; Safaeinili, A.; Ivanov, A.B.; Milkovich, S.M.; Cicchetti, A.; Kofman, W.; Mouginot, J.; Farrell, W.M.; Phillips, R.J.; et al. Subsurface Radar Sounding of the South Polar Layered Deposits of Mars. *Science* **2007**, *316*, 92–95. [CrossRef]
7. Orosei, R.; Lauro, S.E.; Pettinelli, E.; Cicchetti, A.; Coradini, M.; Cosciotti, B.; Di Paolo, F.; Flamini, E.; Mattei, E.; Pajola, M.; et al. Radar evidence of subglacial liquid water on Mars. *Science* **2018**, *361*, 490–493. [CrossRef]
8. Kunimasu, T.; Sawayama, K.; Tsuji, T. Estimation of the mass fraction and distribution of ice in a lunar regolith simulant from seismic velocity. *Icarus* **2023**, *406*, 115725. [CrossRef]
9. Ojha, L.; Wilhelm, M.B.; Murchie, S.L.; McEwen, A.S.; Wray, J.J.; Hanley, J.; Massé, M.; Chojnacki, M. Spectral evidence for hydrated salts in recurring slope lineae on Mars. *Nat. Geosci.* **2015**, *8*, 829–832. [CrossRef]
10. Carter, J.; Riu, L.; Poulet, F.; Bibring, J.-P.; Langevin, Y.; Gondet, B. A Mars orbital catalog of aqueous alteration signatures (MOCAAS). *Icarus* **2023**, *389*, 115164. [CrossRef]
11. Brass, G.W. Stability of brines on Mars. *Icarus* **1980**, *42*, 20–28. [CrossRef]
12. Sears, D.W.G.; Chittenden, J.D. On laboratory simulation and the temperature dependence of the evaporation rate of brine on Mars. *Geophys. Res. Lett.* **2005**, *32*, L23203. [CrossRef]
13. McEwen, S.; Ojha, L.; Dundas, C.M.; Mattson, S.S.; Byrne, S.; Wray, J.J.; Cull, S.C.; Murchie, S.L.; Thomas, N.; Gulick, V.C. Seasonal Flows on Warm Martian Slopes. *Science* **2011**, *333*, 740–743. [CrossRef]
14. Martín-Torres, F.J.; Zorzano, M.-P.; Valentín-Serrano, P.; Harri, A.-M.; Genzer, M.; Kemppinen, O.; Rivera-Valentin, E.G.; Jun, I.; Wray, J.; Madsen, M.B.; et al. Transient liquid water and water activity at Gale crater on Mars. *Nat. Geosci.* **2015**, *8*, 357. [CrossRef]
15. Zorzano, M.-P.; Mateo-Martí, E.; Prieto-Ballesteros, O.; Osuna, S.; Renno, N. Stability of liquid saline water on present day Mars. *Geophys. Res. Lett.* **2009**, *36*, L20201. [CrossRef]
16. Gough, R.V.; Primm, K.M.; Rivera-Valentín, E.G.; Martínez, G.M.; Tolbert, M.A. Solid-solid hydration and dehydration of Mars-relevant chlorine salts: Implications for Gale Crater and RSL locations. *Icarus* **2019**, *321*, 1–13. [CrossRef]
17. Nair, C.P.R.; Unnikrishnan, V. Stability of the Liquid Water Phase on Mars: A Thermodynamic Analysis Considering Martian Atmospheric Conditions and Perchlorate Brine Solutions. *ACS Omega* **2020**, *5*, 9391–9397. [CrossRef]
18. Martín-Torres, J.; Zorzano, M.-P.; Soria-Salinas, Á.; Nazarious, M.I.; Konatham, S.; Mathanlal, T.; Ramachandran, A.V.; Ramírez-Luque, J.-A.; Mantas-Nakhai, R. The HABIT (HabitAbility: Brine Irradiation and Temperature) environmental instrument for the ExoMars 2022 Surface Platform. *Planet. Space Sci.* **2020**, *190*, 104968. [CrossRef]
19. Simon, J.I.; Hickman-Lewis, K.; Cohen, B.A.; Mayhew, L.E.; Shuster, D.L.; Debaille, V.; Hausrath, E.M.; Weiss, B.P.; Bosak, T.; Zorzano, M.-P.; et al. Samples Collected From the Floor of Jezero Crater With the Mars 2020 Perseverance Rover. *J. Geophys. Res. Planets* **2023**, *128*, e2022JE007474. [CrossRef]
20. Tebolt, M.; Levy, J.; Goudge, T.; Schorghofer, N. Slope, elevation, and thermal inertia trends of martian recurring slope lineae initiation and termination points: Multiple possible processes occurring on coarse, sandy slopes. *Icarus* **2020**, *338*, 113536. [CrossRef]
21. Stillman, D.E.; Michaels, T.I.; Grimm, R.E. Characteristics of the numerous and widespread recurring slope lineae (RSL) in Valles Marineris, Mars. *Icarus* **2017**, *285*, 195–210. [CrossRef]
22. Dundas, A.M.; McEwen, A.S.; Chojnacki, M.; Milazzo, M.P.; Byrne, S.; McElwaine, J.N.; Urso, A. Granular flows at recurring slope lineae on Mars indicate a limited role for liquid water. *Nat. Geosci.* **2017**, *10*, 903–907. [CrossRef]
23. Vincendon, M.; Pilorget, C.; Carter, J.; Stcherbinine, A. Observational evidence for a dry dust-wind origin of Mars seasonal dark flows. *Icarus* **2019**, *325*, 115–127. [CrossRef]
24. Stillman, D.E.; Bue, B.D.; Wagstaff, K.L.; Primm, K.M.; Michaels, T.I.; Grimm, R.E. Evaluation of wet and dry recurring slope lineae (RSL) formation mechanisms based on quantitative mapping of RSL in Garni Crater, Valles Marineris, Mars. *Icarus* **2020**, *335*, 113420. [CrossRef]
25. Levy, J. Hydrological characteristics of recurrent slope lineae on Mars: Evidence for liquid flow through regolith and comparisons with Antarctic terrestrial analogs. *Icarus* **2012**, *219*, 1–4. [CrossRef]
26. Strohbeck, P.; Eggenweiler, E.; Rybak, I. A Modification of the Beavers–Joseph Condition for Arbitrary Flows to the Fluid–porous Interface. *Transp. Porous Media* **2023**, *147*, 605–628. [CrossRef]
27. Kakumani, C.; Rath, S.; Terzis, A. Effect of pore-structure on the Beavers-Joseph slip coefficient for a free-flow and porous medium interface. Phys. *Fluids* **2024**, *36*, 062113.
28. Del Mastro, M.; Terzis, A. An experimental investigation of boundary layer over permeable interfaces in Hele-Shaw micromodels. Phys. *Fluids* **2024**, *36*, 112110.
29. Karra, S.K.; Apte, S.V. Numerical investigation of turbulent flow over a randomly packed sediment bed using a variable porosity continuum model. *Phys. Fluids* **2024**, *36*, 115177. [CrossRef]

30. Burt, D.M.; Knauth, L.P. Electrically conducting, Ca-rich brines, rather than water, expected in the Martian subsurface. *J. Geophys. Res. Planets* **2003**, *108*, 8026. [CrossRef]
31. Möhlmann, D.; Thomsen, K. Properties of cryobrines on Mars. *Icarus* **2011**, *212*, 123–130. [CrossRef]
32. Chevrier, V.F.; Rivera-Valentin, E.G. Formation of recurring slope lineae by liquid brines on present-day Mars. *Geophys. Res. Lett.* **2012**, *39*, L21202. [CrossRef]
33. Gough, R.V.; Chevrier, V.F.; Tolbert, M.A. Formation of liquid water at low temperatures via the deliquescence of calcium chloride: Implications for Antarctica and Mars. Planet. *Space Sci.* **2016**, *131*, 79–87. [CrossRef]
34. Toner, J.D.; Catling, D.C. Chlorate brines on Mars: Implications for the occurrence of liquid water and deliquescence. *Earth Planet. Sci. Lett.* **2018**, *497*, 161–168. [CrossRef]
35. Ojha, L.; Wray, J.J.; Murchie, S.L.; McEwen, A.S.; Wolff, M.J.; Karunatillake, S. Spectral constraints on the formation mechanism of recurring slope lineae. *Geophys. Res. Lett.* **2013**, *40*, 5621–5626. [CrossRef]
36. McEwen, A.S.; Dundas, C.M.; Mattson, S.S.; Toigo, A.D.; Ojha, L.; Wray, J.J.; Chojnacki, M.; Byrne, S.; Murchie, S.L.; Thomas, N. Recurring slope lineae in equatorial regions of Mars. *Nat. Geosci.* **2014**, *7*, 53–58. [CrossRef]
37. Marion, G.M.; Kargel, J.S.; Catling, D.C. Modeling ferrous–ferric iron chemistry with application to martian surface geochemistry. *Geochim. Cosmochim. Acta* **2008**, *72*, 242–266. [CrossRef]
38. Cannon, K.M.; Britt, D.T.; Smith, T.M.; Fritsche, R.F.; Batcheldor, D. Mars global simulant MGS-1: A Rocknest-based open standard for basaltic martian regolith simulants. *Icarus* **2019**, *317*, 470–478. [CrossRef]
39. Long-Fox, J.M.; Landsman, Z.A.; Easter, P.B.; Millwater, C.A.; Britt, D.T. Geomechanical properties of lunar regolith simulants LHS-1 and LMS-1. *Adv. Space Res.* **2023**, *71*, 5400–5412. [CrossRef]
40. Dotson, B.; Valencia, D.S.; Millwater, C.; Easter, P.; Long-Fox, J.; Britt, D.; Metzger, P. Cohesion and shear strength of compacted lunar and Martian regolith simulants. *Icarus* **2024**, *411*, 115943. [CrossRef]
41. Ozaki, S.; Ishigami, G.; Otsuki, M.; Miyamoto, H.; Wada, K.; Watanabe, Y.; Nishino, T.; Kojima, H.; Soda, K.; Nakao, Y.; et al. Granular flow experiment using artificial gravity generator at International Space Station. *npj Microgravity* **2023**, *9*, 61. [CrossRef] [PubMed]
42. Tabuchi, Y.; Kioka, A.; Yamada, Y. Water permeability of sunlit lunar highlands regolith using LHS-1 simulant. *Acta Astronaut.* **2023**, *213*, 344–354. [CrossRef]
43. Carrier, W.D.; Olhoeft, G.R.; Mendell, W. Physical properties of the lunar surface. In *Lunar Source Book: A User's Guide to the Moon*; Heiken, G.H., Vaniman, D.T., French, B.M., Eds.; Cambridge University Press: New York, NY, USA, 1991; pp. 530–552.
44. Hayne, P.O.; Bandfield, J.L.; Siegler, M.A.; Vasavada, A.R.; Ghent, R.R.; Williams, J.-P.; Greenhagen, B.T.; Aharonson, O.; Elder, C.M.; Lucey, P.G.; et al. Global Regolith Thermophysical Properties of the Moon From the Diviner Lunar Radiometer Experiment. *J. Geophys. Res. Planets* **2017**, *122*, 2371–2400. [CrossRef]
45. Fa, W. Bulk Density of the Lunar Regolith at the Chang'E-3 Landing Site as Estimated From Lunar Penetrating Radar. *Earth Space Sci.* **2020**, *7*, e2019EA000801. [CrossRef]
46. Imamura, S.; Sekine, Y.; Maekawa, Y.; Kurokawa, H.; Sasaki, T. Effective formation of surface flow due to salt precipitation within soils upon repeated brine seepages on Mars. *Icarus* **2023**, *396*, 115500. [CrossRef]
47. Zhou, M.; Fan, S.; Shi, R.; Yang, Y.; Li, J. Effect of gravity on the mechanical properties of lunar regolith tested using a low gravity simulation device. *J. Terramech.* **2015**, *60*, 11–22. [CrossRef]
48. Schneider, C.A.; Rasband, W.S.; Eliceiri, K.W. NIH Image to ImageJ: 25 years of image analysis. *Nat. Methods* **2012**, *9*, 671–675. [CrossRef]
49. Schindelin, J.; Arganda-Carreras, I.; Frise, E.; Kaynig, V.; Longair, M.; Pietzsch, T.; Preibisch, S.; Rueden, C.; Saalfeld, S.; Schmid, B.; et al. Fiji: An open-source platform for biological-image analysis. *Nat. Methods* **2012**, *9*, 676–682. [CrossRef]
50. Ishii, T.; Kioka, A.; Huang, J.-J.S.; Tabuchi, Y.; Yamada, Y. Low-velocity impact response of lunar and Martian regolith simulants: Implications for lunar and Martian surface explorations. *Phys. Fluids* **2024**, *36*, 113318. [CrossRef]
51. Ishii, T.; Kioka, A.; Huang, J.-J.S.; Tsuji, T.; Yamada, Y. Distinctive impact responses of extraterrestrial regolith simulants: Insights from crater morphology classification and granular dynamics through machine learning and x-ray computed tomography. *Phys. Fluids* **2025**, *37*, 023358. [CrossRef]
52. Costa, A. Permeability-Porosity Relationship: A Reexamination of the Kozeny-Carman Equation Based on a Fractal Pore-Space Geometry Assumption. *Geophys. Res. Lett.* **2006**, *33*, L02318. [CrossRef]
53. Chang, M.-H.; Chen, F.; Straughan, B. Instability of Poiseuille flow in a fluid overlying a porous layer. *J. Fluid Mech.* **2006**, *564*, 287–303. [CrossRef]
54. Beavers, G.S.; Joseph, D.D. Boundary conditions at a naturally permeable wall. *J. Fluid Mech.* **1967**, *30*, 197–207. [CrossRef]
55. Saffman, P.G. On the Boundary Condition at the Surface of a Porous Medium. *Stud. Appl. Math.* **1971**, *50*, 93–101. [CrossRef]
56. Sahraoui, M.; Kaviany, M. Slip and no-slip velocity boundary conditions at interface of porous, plain media. *Int. J. Heat Mass Transf.* **1992**, *35*, 927–943. [CrossRef]

57. Wahab, A.; Mahiuddin, S. Isentropic Compressibility and Viscosity of Aqueous and Methanolic Calcium Chloride Solutions. *J. Chem. Eng. Data* **2001**, *46*, 1457–1463. [CrossRef]
58. Mason, D.P.; Scuderi, L.A. Interweaving recurring slope lineae on Mars: Do they support a wet hypothesis? *Icarus* **2024**, *419*, 115980. [CrossRef]

Disclaimer/Publisher's Note: The statements, opinions and data contained in all publications are solely those of the individual author(s) and contributor(s) and not of MDPI and/or the editor(s). MDPI and/or the editor(s) disclaim responsibility for any injury to people or property resulting from any ideas, methods, instructions or products referred to in the content.